



Original Paper

Experiment and numerical simulation of distribution law of water-based corrosion inhibitor in natural gas gathering and transportation pipeline



En-Bin Liu^{a,*}, Hao Tang^a, Yin-Hui Zhang^{b,c,d}, Dang-Jian Li^e, Bo Kou^a, Ning Liu^a, Mohammadamin Azimi^f

^a Petroleum Engineering School, Southwest Petroleum University, Chengdu, 610500, China

^b Research Institute of Natural Gas Technology, Southwest Oil&Gasfield Company, PetroChina, Chengdu, Sichuan, 610213, China

^c National Energy Research and Development Center of Sour Gas Exploitation, PetroChina, Chengdu, Sichuan, 610213, China

^d Sour Gas Exploitation Pilot Test Center, PetroChina, Chengdu, Sichuan, 610213, China

^e China United Coalbed Methane Corporation, Ltd, Taiyuan, 030000, China

^f Trenchless Technology Center, Louisiana Tech University, Ruston, LA, 71270, USA

ARTICLE INFO

Article history:

Received 15 September 2022

Received in revised form

16 January 2023

Accepted 26 January 2023

Available online 31 January 2023

Edited by Xiu-Qiu Peng

Keywords:

Corrosion inhibitor

Corrosion

Computational fluid dynamics

Electrochemistry

Droplet distribution

ABSTRACT

The transmission medium of natural gas gathering and transportation pipelines usually contains corrosive gases, which will cause serious corrosion on the inner wall of the pipelines when they coexist with water. Therefore, it is necessary to add corrosion inhibitor to form a protective film to protect the pipeline. The distribution of corrosion inhibitors in a gathering and transportation pipeline in Moxi gas field was studied by combining experiment and simulation. The Pearson function was used to calculate the experimental and simulation results, and the correlation was more than 80%, indicating a high degree of agreement. The simulation results show that: ① The larger the pipe angle, filling speed and gas flow rate, the smaller the particle size, the better the distribution of corrosion inhibitor particles in the pipe. The filling amount will affect the concentration, but the distribution trend is unchanged; ② A method to determine the filling mode based on the loss was proposed, and for this pipeline, the loss of corrosion inhibitor was determined to be 5.31×10^{-3} kg/s, and the filling amount was recommended to be adjusted to 20 L/h, which has certain guiding significance for the actual filling strategy of pipeline corrosion inhibitor.

© 2023 The Authors. Publishing services by Elsevier B.V. on behalf of KeAi Communications Co. Ltd. This is an open access article under the CC BY-NC-ND license (<http://creativecommons.org/licenses/by-nc-nd/4.0/>).

1. Introduction

In recent years, with the increase in natural gas demand, its exploitation intensity and utilization degree have been continuously improved (Guo et al., 2022; Wang et al., 2022). Natural gas contains H₂S, CO₂, and other acid gases, which will form acid liquid with free water in the pipeline (Qi et al., 2019). The flow and retention of acid in the pipeline will cause serious corrosion problems, mainly manifested as uniform corrosion, localized corrosion and erosion corrosion. Corrosion inhibitor have the advantages of less dosage, good effect and convenient use, and are widely applied in oil and gas fields, aviation, construction and other

fields (Han et al., 2022; Jaya et al., 2010; Cui et al., 2021). After atomization, the corrosion inhibitor is filled into the pipeline dispersed throughout the pipeline under the influence of gas turbulence and molecular diffusion. However, the corrosion inhibitor droplet itself cannot form a continuous film to protect the pipeline, so the method of refill after pre-filming is generally adopted. The pre-filming process generally uses the pipeline pressure difference to move the pig in the pipeline, and evenly applies the corrosion inhibitor to the inner wall to form a thin continuous film (Jing et al., 2018). Then, the atomized corrosion inhibitor is sprayed into the pipeline by continuous or intermittent filling to supplement the continuous film. The scouring effect caused by the gas flow will lead to problems, such as thinning and destruction of continuous film, reducing the protective effect. Therefore, it is necessary to study the distribution law of corrosion inhibitor to provide technical support

* Corresponding author.

E-mail address: enbin.liu@swpu.edu.cn (E.-B. Liu).

for the pre-filming process. Since it is difficult to obtain the concentration distribution inside the pipeline, the concentration of the corrosion inhibitor is generally detected at the outlet of the pipeline (Rojas and Ojeda, 2009). Scholars at home and abroad have done a lot of research and analysis on corrosion inhibitor, as shown in Table 1.

As can be seen from Table 1, the relevant researches on corrosion inhibitor are mainly divided into two categories. The first category is to analyze the concentration of corrosion inhibitor from a one-dimensional analytical method. For example, Longwell and Weiss (1953) proposed to use the diffusion equation to obtain the concentration distribution downstream of the nozzle. Zheng et al. (1999) corrected Longwell atomization concentration formula and obtained the distribution formula of corrosion inhibitor atomization concentration in natural gas pipelines. Gupta and Torrilhon (2016) study the diffusion velocity in gas mixtures and find a relaxation phenomenon. Due to the limitations of the one-

dimensional analytical method itself, the accuracy of describing the corrosion inhibitor filling process is low. With the development of computational fluid dynamics, many scholars proposed to use the CFD method to establish a model and analyze gas-liquid and gas-solid two-phase flow. For example, Quentin et al. (2021) proposed the influence of surface roughness should be considered when analyzing liquid film in the process of spray formation of liquid film, Yu et al. (2021) according to the atomization characteristics of nozzles, a method for predicting droplet breakage is proposed. Liu et al. (2021a) used the DPM model to study the effect of particles on pipeline erosion and verified that the model can effectively simulate particle motion behaviors. Guan et al. (2015) used the Mixture model to study the liquid transport in natural gas pipelines, and proposed that the liquid film movement is attributed to the combined action of centrifugal force and gravity. Tao et al. (2019) proved that the use of DPM model has certain accuracy by simulating the process of spray formation of the liquid

Table 1
Research status of pipeline corrosion inhibitor.

Analysis perspectives	Results or conclusions	References
One-dimensional	He believed that the liquid after passing through the nozzle would cause a difference in the concentration distribution downstream, and the diffusion equation could be used to find the concentration distribution downstream of the nozzle. By modifying the "Longwell atomization concentration formula", the distribution formula of the corrosion inhibitor atomization concentration in the natural gas pipeline is obtained, and the undetermined constants in the formula are corrected. By studying the atomization distribution of the corrosion inhibitor in the pipeline, it is proposed that a set of modified "Longwell diffusion models" is established based on the theory of gravity settlement and relaxation, and the experimental deviation of which is small. The study is carried out on diffusion velocity and relaxation in binary gas mixtures by Boltzmann collision integral. The corrosion inhibition performance of imidazoline derivatives on J55 steel in oilfield formation water saturated with CO ₂ was studied. The addition of corrosion inhibitor reduces the current density of the cathode and anode and improves the impedance parameters.	Longwell et al. (1953) Zheng et al. (1999) Jing et al. (2018) Gupta et al. (2016) Singh et al. (2019)
Three-dimensional	Inhibition effect of thioureidoimidazoline inhibitor for the flow accelerated corrosion at different locations of X65 carbon steel elbow was studied by array electrode and computational fluid dynamics simulation. The liquid transport and film flow in a low-pressure natural gas pipeline are studied by using a mixture model. It is proposed that the formation of liquid film and the movement of droplets are attributed to centrifugal force and gravity. The diffusion process of liquid film formed by high pressure spray on a flat plate was studied. The influence of liquid film is analyzed from many angles. According to the atomization characteristics of the nozzle, a method for predicting droplet rupture was proposed, and its practicability was verified by experiments. The corrosion behavior of cross section with variable diameter was studied by computational fluid dynamics (CFD) method, and the relationship between the flow rate and corrosion rate was determined by experiments. The overflow phenomenon in an inclined pipe is studied, and the simulation results verify that the model can provide a deeper understanding of the liquid film structure in the gas-liquid two-phase flow than the experiment.	Zeng et al. (2015) Guan et al. (2015) Quentin et al. (2021) Yu et al. (2021) Zhong et al. (2020) Chen et al. (2015)
Three-dimensional	The Discrete phase model (DPM) was adopted to study the effect of particles on pipeline erosion, and it was verified that the model can effectively simulate particle movement behaviors. The newly developed model is used to simulate the powder prepared by gas atomization, and visualize the continuous liquid and droplet crushing and defect formation process. Based on the CFD method, a numerical calculation program is established to obtain the specific film thickness of the elbow through the mechanical film model. Volume of Fluid (VOF) and Euler-Euler method is used to simulate the three-dimensional transient annulus. It is proposed that the liquid film in three-phase flow is helpful to reduce the erosion damage, compared with that in two-phase flow. By simulating the liquid disintegration process in the three-phase system, a new numerical simulation method of liquid jet spraying in the nozzle is proposed, and the feasibility of such a method is verified by comparison. The gas-liquid separation process in axial flow cyclone is simulated by combining the Euler-Lagrange method with the surface film model. The surface droplets will move to the wall under the action of centrifugal force to form a thin liquid film. The discrete phase model is combined with the boundary conditions of the wall film to simulate the liquid atomization and spray process, and the influence of different parameters on the liquid film is analyzed. The simulation results are compared with the experimental data in the literature. The error is small. CFD method is used to analyze the perforation failure of atmospheric distillation column pipeline system, and provide theoretical guidance. The effects of bubble detachment time and particle entrainment under the wettability of gas nozzle materials were investigated using DPM and VOF models. Aiming at the serious corrosion problem of gas collecting station, the distribution mechanism of liquid film was analyzed by establishing the model of Euler wall film and multiphase flow. Regarding the liquid load problem caused by insufficient gas production in the wellbore of gas wells, the CFD method is used to simulate the relationship between liquid film reversal and gas flow rate in a two-phase co-current annular pipeline. The theoretical model of VOF and continuous surface force is adopted to discuss the interfacial movement, exploring the liquid dispersion and film properties of the horizontal tubes under spray impact.	Liu et al. (2021a) Luo et al. (2021) Liu et al. (2019) Farokhipour et al. (2020) Edelbauer. (2017) Deng et al. (2019) Tao et al. (2009) Quan et al. (2022) Xu et al. (2013) Liu et al. (2022a) Adaze et al. (2019) Lee et al. (2020)
Three-dimensional	By establishing a CFD model of atomized stratified flow, the transport of water droplets in the gas-liquid multiphase system in large-diameter pipes is studied.	Verdin et al. (2014)

film. To sum up, many scholars have used the CFD method to simulate the internal flow of the pipeline, but there is a lack of corresponding experiments to verify the accuracy. Especially for the research on the distribution of corrosion inhibitor, most scholars only carried out a single experiment or simulation. Therefore, this study adopts the method of combining numerical simulation and experiment to study the distribution law of corrosion inhibitor in 3D flow field, and provides certain technical support for on-site corrosion inhibitor process and pipeline safe operation (Liu et al., 2022b, 2022d).

This paper independently designed a set of experimental equipment to analyze the field corrosion inhibitor process, through the analysis of the filling process and then put forward the optimization and improvement measures, simulation analysis of the corrosion inhibitor loss under the pre-film process, and combined with the independent programming software to propose a filling strategy different from the field experience formula. In the second part of the article, the experimental part is introduced, including experimental equipment and testing methods. And using the Pearson function in statistics, the corrosion inhibitor concentration in the simulation results is linked with the electrochemical impedance spectroscopy experiment and the polarization curve, and the correlation between the two is calculated to verify the accuracy of the simulation. The third part mainly introduces the model and model parameters in the actual case. The fourth part mainly combines the Mixture model and the DPM model according to the field process to simulate the distribution law of corrosion inhibitor injection under the influence of different factors, and analyze the selection of corrosion inhibitor loss and injection method under the pre-coating process.

2. Experiment and model validation

The corrosion inhibitor is atomized by the storage tank and passed into the pipeline under the action of pump pressure, and then adsorbed on the pipe wall to form a protective film to slow down the corrosion of the pipeline. In this part, parameters such as electrode impedance value and corrosion current at different positions are obtained by electrochemical experiments, and correlation analysis with numerical simulation corrosion inhibitor concentration is carried out to find a suitable calculation model.

2.1. Experimental setup and testing

2.1.1. Experimental device

By combining the on-site corrosion inhibitor filling conditions, a

set of experimental equipment to simulate the distribution of corrosion inhibitor in gathering and transportation pipelines was independently designed, as shown in Fig. 1. The material of the pipe selected for the experimental device is organic glass. The specifications of the pipe are the outer diameter (D) of 30 mm, the wall thickness of 5 mm, the radius of curvature of the elbow 45 mm (1.5D), the length of the uphill section of 1 m, and the length of the horizontal section 2 m. According to the simulation results, holes are drilled in different positions of the pipeline, and the working electrodes made of L360 carbon steel are installed and taken out for electrochemical test after continuous feeding of the corrosion inhibitor. The gas in the experiment is generated by the air compressor, and the moisture in the air is removed by the refrigerated dryer. After the corrosion inhibitor is atomized by the porous ultrasonic atomization system (⑤), it is sucked and carried by the Venturi proportional mixer (⑥) to the tube to form a film. The device can perform experiments such as corrosion inhibitor apparent experiment, electrochemical experiment and surface analysis.

2.1.2. Experimental steps

The corrosion inhibitor used in this experiment is mainly composed of compounds with sulfur containing imidazoline as the main material and water as the auxiliary material. Its concentration in the experiment is controlled at 500 mg/L. By drilling holes and installing electrodes in multiple locations of the experimental pipeline, electrochemical impedance and polarization curve tests were performed to evaluate the effect of the inhibitor (as shown in Fig. 2), and the distribution results were compared with the three-dimensional numerical simulation results to verify the accuracy of the model.

Firstly, start the inhibitor atomization system, and open the air compressor to continuously fill the experimental gas. Take out the electrodes at different positions, in turn, dry them at room temperature of 25 °C, and put them into a four-mouth flask together with the reference electrode and auxiliary electrode for the experimental test to obtain the resistance value and corrosion current intensity at different positions of the pipeline. Specifically, the electrochemical impedance spectrum is fitted by ZView2 and ZSimDemo software, with the scanning speed of the polarization curve of 0.5 mV/s, the sinusoidal alternating amplitude 10 mV, and the frequency from 1×10^5 Hz–0.05 Hz.

2.1.3. Model validation

By extracting the corrosion inhibitor concentration at different positions in the numerical simulation, the impedance value of the

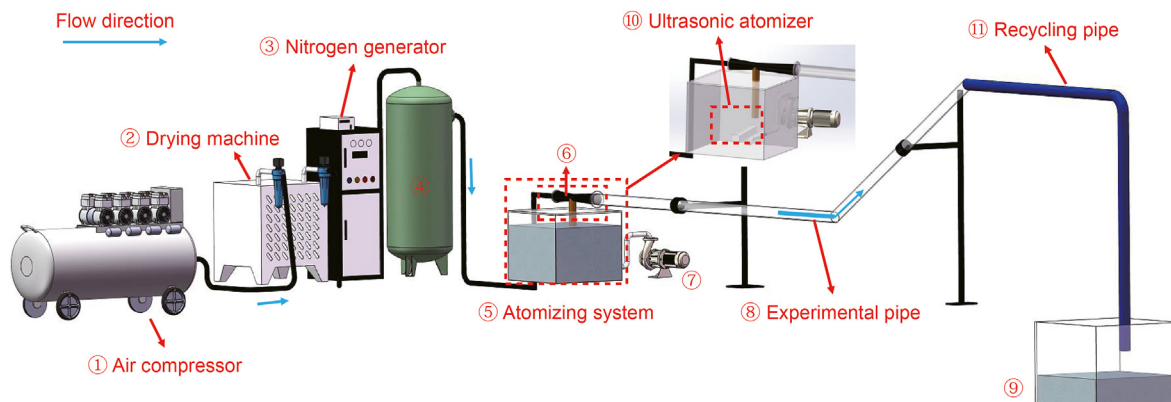


Fig. 1. Experimental device.

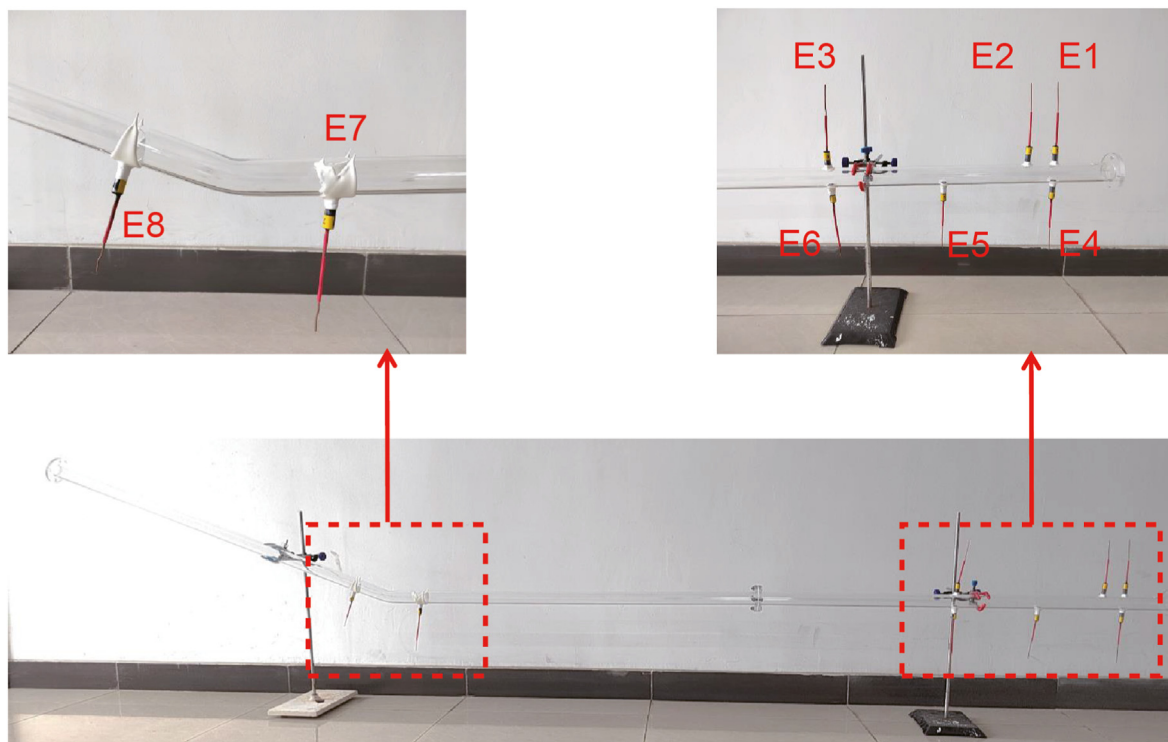


Fig. 2. Electrode punching position.

electrochemical test and the corrosion current are analyzed for correlation, and the model is numerically verified. The test results of AC impedance spectrum were fitted using the circuit diagram shown in Fig. 3, and the fitting errors were shown in Table 2.

According to the relationship between OCP and time shown in Fig. 4, when the time was in the 1800s, the OCP of each group was stable, indicating that the corrosion inhibitor had been adsorbed on the electrode surface and was in a state of equilibrium. Therefore, this time was used in the subsequent experiments. The electrochemical test results are shown in Fig. 5. For the polarization curve, the stable E_{ocp} value ± 0.25 V is usually used as the measurement range of the Tafel curve, and the scanning speed is 0.5 mV/s. The linear part of the logarithmic Tafel plot is extrapolated to intersect at a point, which is defined as an approximation of the corrosion current i_{corr} and the corresponding corrosion potential E_{corr} . Eq. (1) is used to calculate the corrosion inhibition rate (η) (Chai et al., 2020), and the results of which are shown in Table 2.

$$\eta = \frac{i_{corr}^0 - i_{corr}^i}{i_{corr}^0} \times 100\% \tag{1}$$

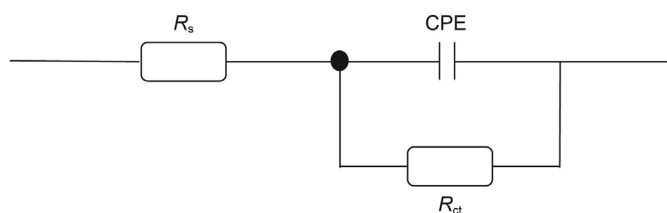


Fig. 3. EIS fitting circuit diagram.

where i_{corr}^0 represents the corrosion current density in the absence of corrosion inhibitor, $\mu\text{A}/\text{cm}^2$, i_{corr}^i is the corrosion current density in the presence of corrosion inhibitor, $\mu\text{A}/\text{cm}^2$.

It can be seen from Table 2 that the charge transfer resistance R_{ct} increases significantly after adding the corrosion inhibitor compared with the blank experiment. It shows that the corrosion inhibitor has a good inhibitory effect on the corrosion of carbon steel. The impedance value of the blank group was $147.1 \Omega \cdot \text{cm}^2$ and the impedance value of the No. 3 electrode was $139.4 \Omega \cdot \text{cm}^2$, which had no significant difference, indicating that there was no corrosion inhibitor at the No. 3 electrode. According to the measured data of the remaining electrodes, it can be found that with the increase of the corrosion inhibitor concentration, the impedance value of each electrode also increases, and the extreme value of impedance $955.5 \Omega \cdot \text{cm}^2$ appears at the No. 6 electrode. Since there is no corrosion inhibitor at the No. 3 electrode position, there is no significant difference in the corrosion current between the No. 3 electrode and the blank group, and the calculated corrosion inhibition rate can be considered to be caused by experimental errors. The corrosion inhibitor concentration is the largest at the No. 6 electrode, the corrosion current measured in the experiment is $8.80 \mu\text{A}/\text{cm}^2$, and the corrosion inhibition rate reaches 91.1%, indicating that the electrochemical corrosion reaction rate on the electrode surface is significantly slowed down.

The three-dimensional calculation model of the test pipe section is established. The pipe angle is 15° , the length of the straight pipe section is 2 m, the length of the uphill section is 1m, and the bending radius (R_c) is 45 mm. In this paper, the Mixture model of multiphase flow and the discrete phase model in the computational fluid dynamics software Fluent were used for coupled calculations, and the RNG $k-\epsilon$ model was chosen for the turbulence model. The selected model is described later. The gas flow rate is 2 m/s, the gas density is $1.225 \text{ kg}/\text{m}^3$, and the viscosity is $1.7894 \times 10^{-5} \text{ kg}/(\text{m} \cdot \text{s})$. By measuring the quality difference of corrosion inhibitor before

Table 2
Electrochemical test results and corrosion inhibition rate.

Electrode	R_{ct} , $\Omega \cdot \text{cm}^2$	Error, %	Corrosion current density i_{corr} , $\mu\text{A}/\text{cm}^2$	Corrosion inhibition rate η , %
Blank	147.1	0.48	99.76	–
1	470.0	0.82	31.52	68.4
2	279.8	1.07	58.51	41.3
3	139.4	6.04	91.25	8.5
4	395.9	4.7	34.55	65.4
5	681.9	1.40	21.97	78.0
6	955.5	1.72	8.80	91.1
7	507.5	3.10	29.67	70.3
8	323.6	0.87	44.23	55.7

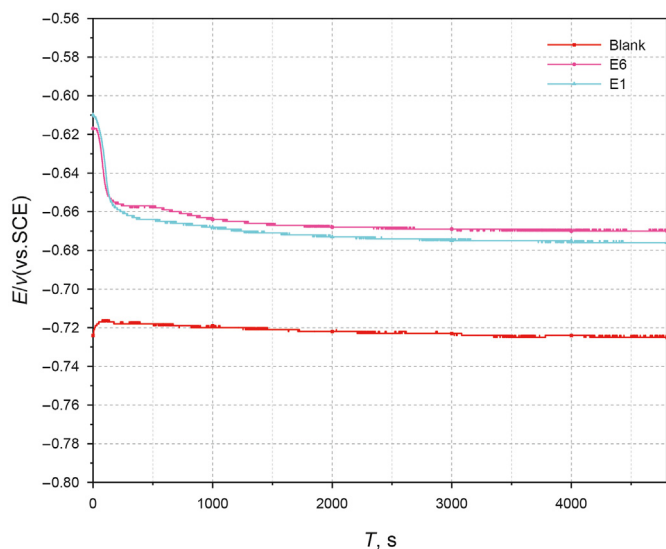


Fig. 4. Relationship between OCP and time.

and after the experiment, the injection quantity of corrosion inhibitor is 3.3×10^{-5} kg/s, and the particle size conforms to the Rosin-Rammler distribution of 0.1–10 μm . Pearson function in statistics was adopted to analyze the correlation between the concentration of corrosion inhibitor at each electrode and the impedance value in electrochemical test and the corrosion current respectively. The error between the corrosion inhibitor concentration and the electrochemical impedance value is 2%. Since the addition of corrosion inhibitor can inhibit the negative and anode of the electrochemical corrosion reaction (Meeusen et al., 2020), the concentration of corrosion inhibitor is negatively correlated with the corrosion current. Therefore, the absolute value is taken as the correlation between the two, that is, the correlation is 80%, as shown in Fig. 6. The simulation results were verified by electrochemical test of corrosion inhibitor, and the correlation between simulation and experiment was high, that is, the simulation results had high credibility.

3. Case introduction

3.1. Model and simulation parameters

A gathering pipeline in Moxi was put into operation in July 2014, and the current starting pressure of the pipeline is 7.35 MPa. Combined with the routing conditions provided on site, taking a 15° pipe section as an example, the calculation model is shown in Fig. 7. The diameter of the pipe (D) is 0.273 m, the length of the

straight pipe section and the uphill section are both 20 m, the radius of curvature of the elbow (R_c) is 0.4095 m, and the curvature ratio (R_c/D) is 1.5. To make the simulation results closer to the actual situation, it should be ensured as much as possible that the calculation model conditions are consistent with the parameters of the gathering pipeline during operation. The setting of key parameters of the pipeline calculation model are shown in Table 3.

3.2. Mathematical model

3.2.1. Multiphase flow model

The Mixture model is a simplified multiphase flow model. The continuous phase can be fluid or particles and is regarded as a continuum interspersed with each other. It is suitable for studying low-load particle flow and sedimentation processes interspersed between the two phases. In this study, there is a certain velocity difference between the gas and liquid phases in the field, and the corrosion inhibitor droplets will mix with the liquid phase in the multiphase flow. Therefore, combined with the field conditions, it is found that the Mixture model is more in line with the simulation requirements.

Assuming that the volume deformation rate of the fluid in the tube is 0, that is, the fluid is incompressible, the continuity equation of the Mixture model is as follows (Bagheri and Sari, 2022).

$$\frac{\partial}{\partial t}(\rho_m) + \nabla \cdot (\rho_m \vec{v}_m) = 0 \tag{2}$$

$$\vec{v}_m = \frac{\sum_{k=1}^n \alpha_k \rho_k \vec{v}_k}{\rho_m} \tag{3}$$

$$\rho_m = \sum_{k=1}^n \alpha_k \rho_k \tag{4}$$

where ρ_m is the average density of the mixed-phase; \vec{v}_m is the average velocity of the mixed-phase; α_k the volume fraction of the k phase; \vec{v}_k the velocity of the k phase; n the number of phases; $\sum_{k=1}^n \alpha_k = 1$. The momentum equation of the Mixture model is as follows.

$$\nabla \cdot (\rho_m \vec{v}_m \vec{v}_m) = -\nabla p + \nabla \cdot [\mu_m (\nabla \vec{v}_m + \vec{v}_m^T)] + \rho_m \vec{g} + \vec{F} + \nabla \cdot \left(\sum_{k=1}^n \alpha_k \rho_k \vec{v}_{dr,k} \vec{v}_{dr,k} \right) \tag{5}$$

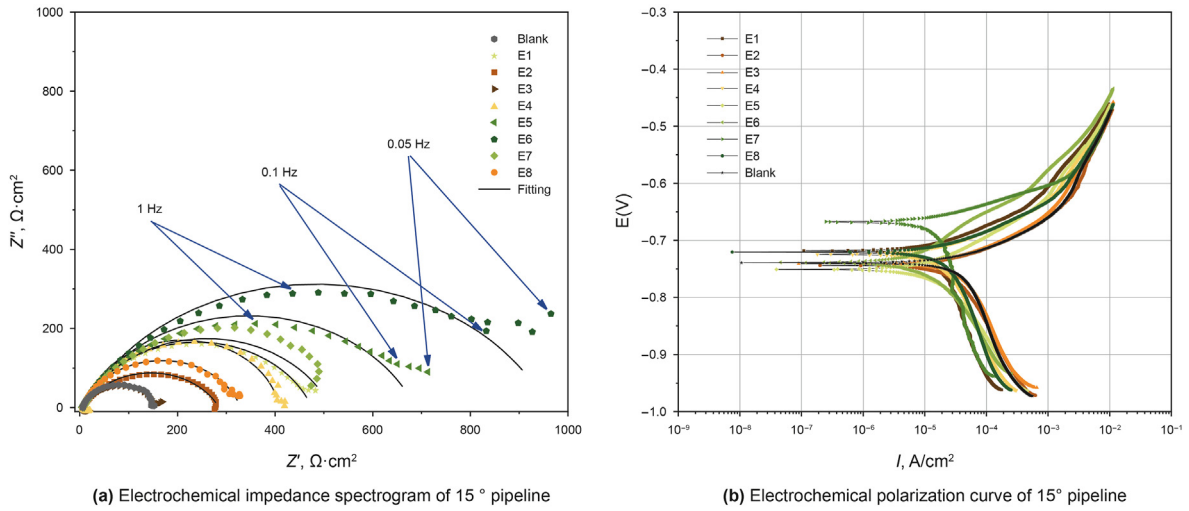


Fig. 5. Test results of pipes with an inclination of 15°

$$\mu_m = \sum_{k=1}^n \alpha_k \mu_k \quad (6)$$

$$\vec{v}_{dr,k} = \vec{v}_k - \vec{v}_m \quad (7)$$

where $\rho_m \vec{g}$ and \vec{F} are the gravitational body force and the external body force, respectively; μ_m is the mixing viscosity coefficient; $\vec{v}_{dr,k}$ the drift velocity of the k -phase.

3.2.2. Discrete phase model

Due to the small volume fraction of the simulated corrosion inhibitor droplet particles, the discrete phase model (DPM) and Euler-Lagrange method are used to simulate the flow field and monitor the droplet trajectory (Li et al., 2018; Chen et al., 2022). The equation of motion of discrete phase particles is expressed as follows.

$$\frac{du_p}{dt} = F_D(u - u_p) + \frac{g(\rho_p - \rho)}{\rho_p} + \Sigma f_p \quad (8)$$

where $F_D(u - u_p)$ is the drag force in per unit mass of corrosion inhibitor droplet, N; u and u_p are respectively the stream velocity and the corrosion inhibitor droplet velocity, m/s; g the gravitational acceleration, m/s²; ρ_p and ρ respectively the inhibitor density and the gas phase density, kg/m³; f_p the other forces on per unit mass droplets, N.

3.2.3. Turbulence model

In this study, when using Fluent to calculate turbulence, the effects of turbulent kinetic energy and turbulent dissipation rate are considered. The accuracy of the RNG $k-\epsilon$ model is improved due to the addition of a condition to the standard $k-\epsilon$ and has higher confidence and accuracy in a wide range of flows (Mompean, 1998; Liu et al., 2022c). It is in line with the complex situation of the distribution of corrosion inhibitor in the gathering pipeline in this

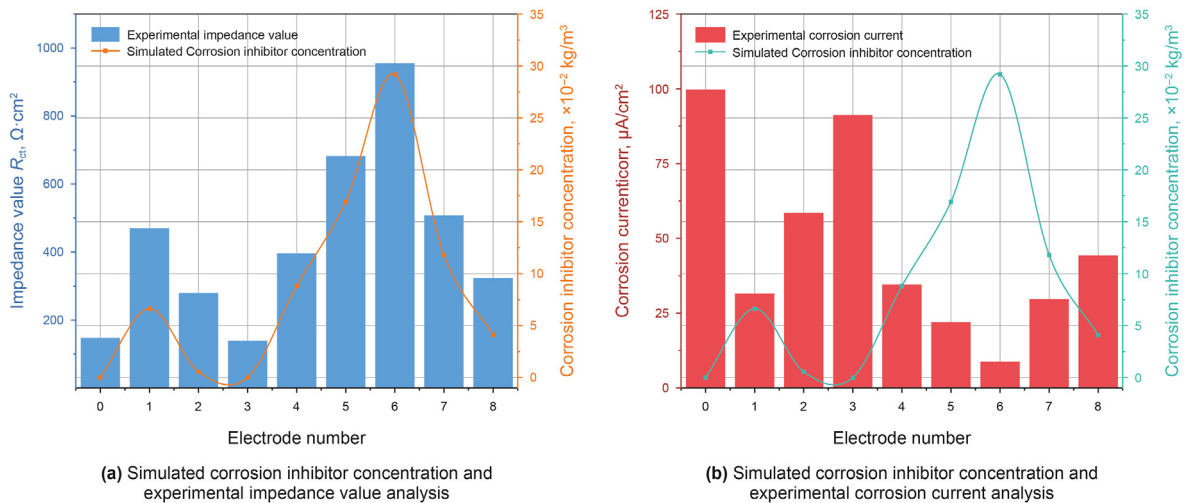


Fig. 6. Correlation analysis between simulation and experimental results.

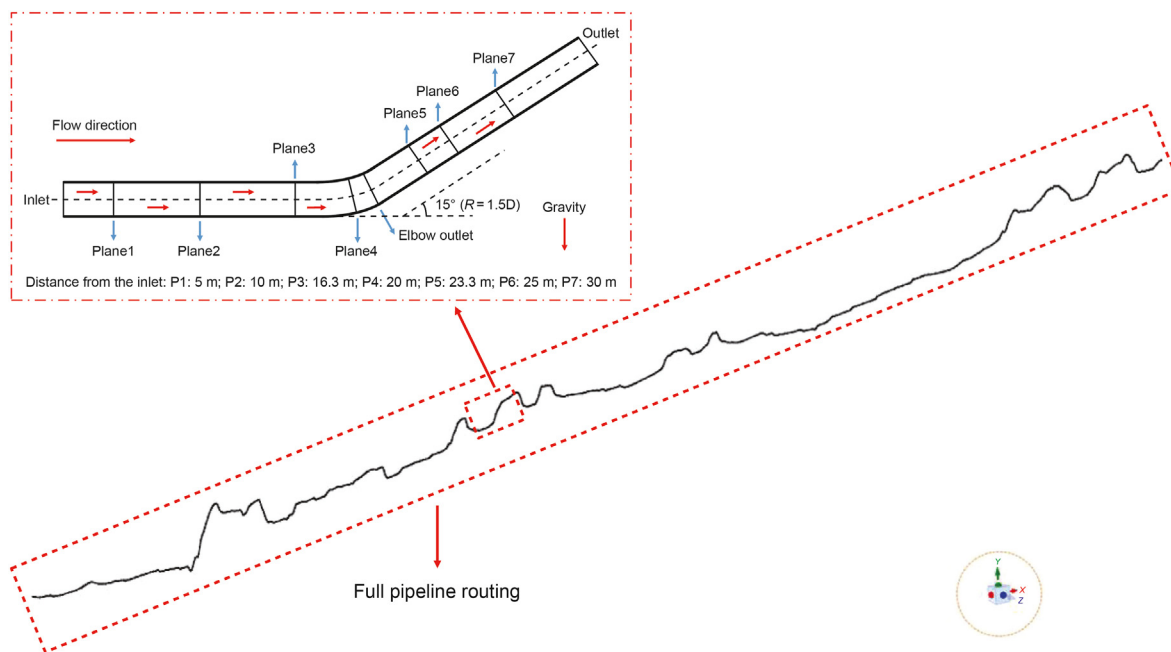


Fig. 7. Computational model diagram.

Table 3
Setting of key parameters.

Parameter	Numerical value
Gas phase density	0.6679, kg/m ³
Liquid Density	998.2, kg/m ³
Corrosion inhibitor particle size	1–20, μm(Rosin-Rammler)
Corrosion inhibitor filling volume	0.00148, kg/s
Pipe diameter	273, mm
Pipeline pressure	7, MPa
Liquid content	0.074

study. The turbulent flow equation is as follows.

$$\rho u_i \frac{\partial k}{\partial x_i} = \frac{\partial}{\partial x_j} \left[\left(\mu + \frac{\mu_t}{\sigma_k} \right) \frac{\partial k}{\partial x_j} \right] + G_k - \rho \epsilon \tag{9}$$

$$\rho u_i \frac{\partial \epsilon}{\partial x_i} = \frac{\partial}{\partial x_j} \left[\left(\mu + \frac{\mu_t}{\sigma_\epsilon} \right) \frac{\partial \epsilon}{\partial x_j} \right] + C_{1\epsilon} G_k \frac{\epsilon}{k} - C_{2\epsilon} \rho \frac{\epsilon^2}{k}$$

$$\mu_t = \rho C_\mu \frac{k^2}{\epsilon} \tag{10}$$

where k is the TKE, ϵ is the TKE dissipation rate, G_k is the generation of turbulent kinetic energy due to the mean velocity gradients, μ_t the turbulent viscosity. According to the renormalization group (RNG) theory, by default $C_{1\epsilon} = 1.42$, $C_{2\epsilon} = 1.68$.

3.2.4. Boundary condition setting

Given the flow rate and outlet pressure in the pipe, the inlet surface is set to velocity-inlet and the outlet condition is set to pressure-outlet. By default, all variables are evenly flowing, and the mixture model in the multiphase flow is selected to simulate the continuous phase (Peng et al., 2021). In the actual working condition, under the action of pump pressure, the atomized corrosion inhibitor is sprayed into the pipe through the nozzle, and the less volume can meet the anticorrosion requirements, so the DPM model is used to simulate the corrosion inhibitor. The corrosion inhibitor

will settle in the pipe until a film is formed on the pipe wall. The no-slip wall is selected, and the boundary condition is set as a trap.

3.2.5. Solving algorithm

The finite volume method (FVM) is used to discretize the control volume, and Fluent is used as the numerical solver. In the solution process, the pressure-based implicit solution is selected, the flow is steady, the SIMPLE algorithm is used to couple the pressure and velocity, and the Second Order Upwind discrete format is used for the momentum, turbulent kinetic energy, and turbulent dissipation rate to improve the calculation accuracy (Liu et al., 2021b). Due to the effect of liquid surface tension, the implicit body force is considered to improve the convergence of the solution.

3.3. Meshing and independence verification

The gas-liquid two-phase flow is mainly in the natural gas gathering and transportation pipeline, where the flow situation is very complicated. The domestic corrosion inhibitor process requires the formation of a protective film with a thickness of 0.1–0.2 mm on the inner wall of the pipeline. As the flow of the corrosion inhibitor film is along the wall, the boundary layer division of the grid near the wall of the pipeline is beneficial to capturing the flow characteristics near the fluid boundary. Since the flow velocity at the elbow of the pipeline changes greatly, to ensure that the numerical simulation results are more in line with the actual situation, it is necessary to divide the calculation model reasonably. The structured grid is selected to mesh all the models used. Taking the 15° elbow as an example, under the parameters in Table 3, the maximum inhibitor concentration on the wall and the center concentration of plane 6 are selected as indicators to verify the independence of the grid. The results are shown in Table 4. When the number of grids reaches 4,028,665, the error of the maximum inhibitor concentration is only 1×10^{-6} , meeting the requirements of grid independence. The grid division is shown in Fig. 8.

4. Results and discussion

4.1. Analysis of internal flow field in pipeline

Although the geometric model of the elbow is relatively simple, the internal flow pattern of the elbow is very complex. According to the Bernoulli equation, when the fluid passes through the outside of the elbow, the fluid velocity decreases and the static pressure increases, and the changing trend on the inside of the elbow is opposite to that on the outside. Under the joint action of centrifugal force field and pressure gradient, a secondary flow, also known as Dean vortex, will flow from the outside to the inside near the wall. To analyze the influence of the internal flow field of the pipeline on the distribution of the corrosion inhibitor, the section at the middle of the elbow and the outlet of the elbow at different angles are selected for analysis, as shown in Fig. 9 (a, c, and e are the middle of the elbow at 10°, 15°, and 20°, respectively, b, d, and f are the elbow outlet at 10°, 15°, and 20°, respectively). It can be seen from Fig. 9 that the existence of the vortex makes the corrosion inhibitor settled at the bottom of the pipe at the end of the straight pipe section to be carried up again, so that the distribution of the corrosion inhibitor passing through the elbow gradually tends to be uniform. With the increase of the pipe angle, the maximum gas velocity in the middle of the head gradually moves upward, and demonstrates an increasing trend at 20°. The corrosion inhibitor at the bottom of the pipe follows the gas flow, and the vortices at different positions at the same angle show the vortex moving to both sides, and the vortex core tends to become smaller.

4.2. Analysis of influencing factors of the continuous filling process

4.2.1. Influence of pipeline angle on corrosion inhibitor distribution

According to the situation of the pipeline, the undulation angle of the whole pipeline is 0–20°, and the influence of different angles (5°, 10°, 15°, 20°) on the distribution of the corrosion inhibitor is considered. In the case of the angles of 15°, with the continuous phase of methane and water, the DPM model is adopted. The gas flow rate is 7 m/s, the liquid flow rate 1.5 m/s, and the filling volume of the corrosion inhibitor 6 L/h. To observe the distribution of corrosion inhibitor in the 15° pipeline more intuitively, the pipe wall is selected as the research object to observe the distribution of corrosion inhibitor, as shown in Fig. 10.

It can be seen from Fig. 10 that the concentration of the corrosion inhibitor at the pipe wall varies greatly, and only some pipe sections have the feature of uniform distribution of the corrosion inhibitor along the circumference of the pipe. As the flow distance gradually increases, the concentration of the inhibitor at the top of the pipe decreases continuously. When the fluid passes through the elbow, the corrosion inhibitor rises again, causing the concentration of the corrosion inhibitor in the upper part of the pipeline to increase rapidly, and then decrease with the increase of the flow distance. Since the fluid is affected by gravity during the flow, the corrosion inhibitor continues to settle, causing the concentration of the inhibitor at the bottom of the pipeline to be much greater than that at the top. When the fluid flows through the elbow, the influence of the secondary flow gradually increases, resulting in a large increase in the concentration of the corrosion inhibitor in the upper part of the pipeline.

To analyze the corrosion inhibitor concentration inside the pipeline, a total of 9 sections as shown in Fig. 7 were selected to analyze the distribution of the corrosion inhibitor concentration in each section, as shown in Fig. 11.

According to the analysis in Fig. 11, the corrosion inhibitor is sprayed in the form of a surface from the inlet, and a uniform annular protective film is formed at the inlet. In the straight pipe

section, due to the influence of gravity, the corrosion inhibitor sprays gradually settles. The larger particle settles first in the front part of the pipe, while the smaller particle follows the airflow. The maximum value of the corrosion inhibitor at the cross-section appears at the bottom of the pipeline, and the concentration distribution of the corrosion inhibitor at other positions is more uniform. However, when the fluid passes through the elbow, the concentration of the corrosion inhibitor at the top of the pipeline decreases sharply, at the same time, in the upslope section of the pipeline, the distribution of the corrosion inhibitor shows a "groove" shape, and the peak value of the corrosion inhibitor appears in the section near the elbow in the upper half of the pipe. This is due to the phenomenon of secondary flow after passing through the elbow which causes the corrosion inhibitor settled at the bottom of the straight pipe section to be carried up to the middle and upper part of the pipeline, while the corrosion inhibitor accumulates in the middle and lower part of the farther section.

To further analyze the distribution of corrosion inhibitor at different angles, some planes (Plane 4, Plane 5, Plane 6) at other angles are selected for demonstration, and the cloud diagram of the corrosion inhibitor distribution is shown in Fig. 12.

According to Fig. 12, as the angle of the pipe increases, the distribution of the corrosion inhibitor in the pipe is gradually uniform. And it can be seen from b, e and h that when the angle of the pipeline rises from 5° to 20°, the extent of the rise of the corrosion inhibitor in the section after passing through the elbow also gradually increases. It is shown that the maximum value of the corrosion inhibitor concentration in the section basically appears at the top of the pipeline and gradually moves upward, and the concentration in the middle and lower parts decreases accordingly. This is because the secondary flow carries the corrosion inhibitor from the bottom to the middle and upper parts after passing through the elbow.

To further observe the distribution of inhibitor concentration along the circumference of the pipeline, Plane 2 and Plane 5 at different angles are extracted for analysis. The selection rule followed the right-hand rule. The direction is determined by 12 points of the clock on the pipe wall, and 12 points represent 0°, as shown in Fig. 13. The calculation results were imported into the post-processing software, and the concentration of the corrosion inhibitor at the section is extracted to establish a radar chart, as shown in Fig. 14.

It can be seen from Fig. 14 that the concentration of the corrosion inhibitor on the wall is concentrated at 90°–270° at the position of the straight pipe 10 m away from the inlet, and the concentration is higher at the bottom of the straight pipe. Under the influence of gravity, the corrosion inhibitor of the upper part settles to the middle and lower parts. It can be seen from Plane 5 of all angles that parts of the corrosion inhibitor settled at the bottom are carried up to the middle and upper part of the pipeline after passing through the elbow due to the secondary flow. With the increase of the pipeline angle, the concentration distribution of the corrosion inhibitor is more uniform. After the 20° pipeline elbow, the corrosion inhibitor settled at the bottom of the pipe is strongly affected by the secondary flow intensity, resulting in the uniform distribution of the corrosion inhibitor in the entire circumference at Plane 5.

4.2.2. Influence of filling volume on the distribution of corrosion inhibitor

The volume of corrosion inhibitor filled directly affects the concentration contained in the pipe wall, thereby affecting the corrosion rate. The distribution of corrosion inhibitor in the pipeline is numerically simulated under different filling rate conditions. According to the field data, the influence of the corrosion inhibitor

Table 4
Grid independence verification.

Grid number	1827319	2484275	3116995	4028665	5809468	6305832
Maximum inhibitor concentration, kg/m ³	0.017913	0.018563	0.020963	0.020968	0.020967	0.020968
error	14.57%	11.40%	0.024%	—	0.005%	0
Plane6 DPM Concentration, kg/m ³	0.001877	0.001983	0.002017	0.002049	0.002049	0.002050
error	8.394%	3.22%	1.56%	—	0	0.05%

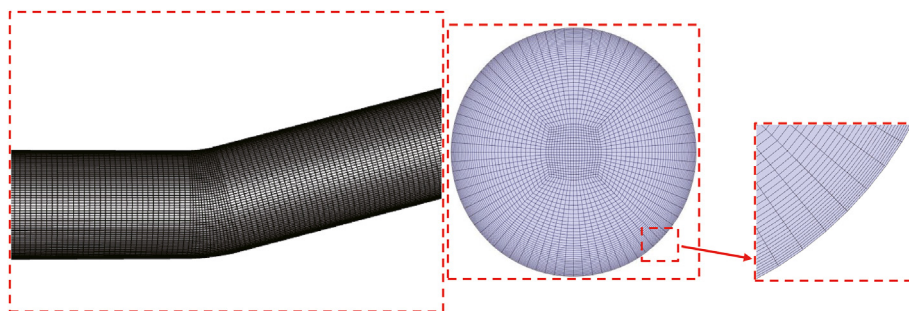


Fig. 8. Grid division diagram.

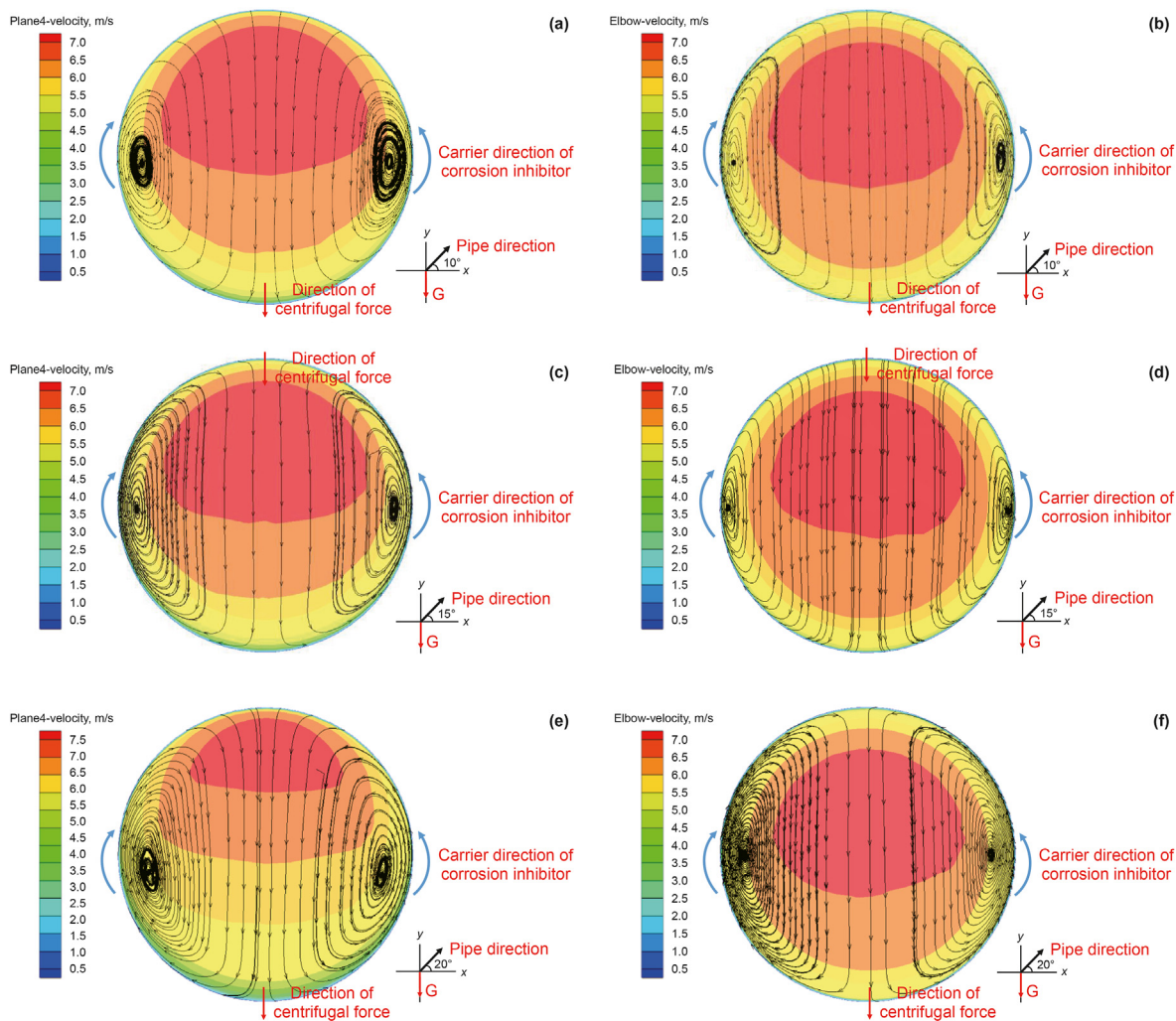


Fig. 9. Cross-sectional streamline diagram.

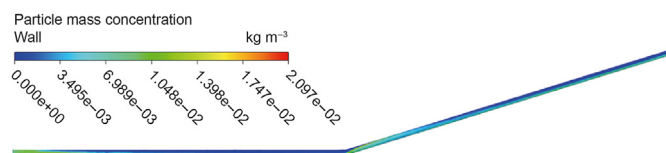


Fig. 10. Concentration distribution of corrosion inhibitor on the pipe wall.

filling volume on its distribution is analyzed after increasing from 5 L/h to 15 L/h. The extracted data points are 0.15 mm above and below the pipe wall, and a point is extracted every 3 m, as shown in Fig. 15. Corrosion inhibitor concentration at each point is shown in Fig. 16.

It can be seen from Fig. 16(a) that under the same filling volume, the corrosion inhibitor concentrations at the upper and bottom parts gradually decrease, and the gas turbulence causes a local small-scale rise, but the overall trend gradually decreases. When

the filling volume increased from 5 L/h to 15 L/h, with the increase of the corrosion inhibitor filling volume, the concentration at each extraction point increases correspondingly, showing a positive correlation. It is indicated that the increase of the filling volume will increase the concentration of the corrosion inhibitor in the pipe, but the distribution trend of the corrosion inhibitor is basically unchanged.

4.2.3. Influence of gas flow rate on inhibitor distribution

The flow rate of pipeline gas is an important factor affecting the distribution of corrosion inhibitor. In this section, the flow field and distribution problems are analyzed under different flow rates of the pipeline and the gas flow rate ratio is 3–9 m/s. For the particle size, the R-R distribution (Rossing-Lammler distribution) is adopted, with the maximum particle size of 20 μm, the minimum particle size of 1 μm, and the average of 9 μm. The parameters such as the filling volume are set according to Table 3, and the concentration of the corrosion inhibitor at each point is extracted for analysis. The obtained curve is shown in Fig. 17.

As can be seen from Fig. 17(a), with the increase of flow rate, the

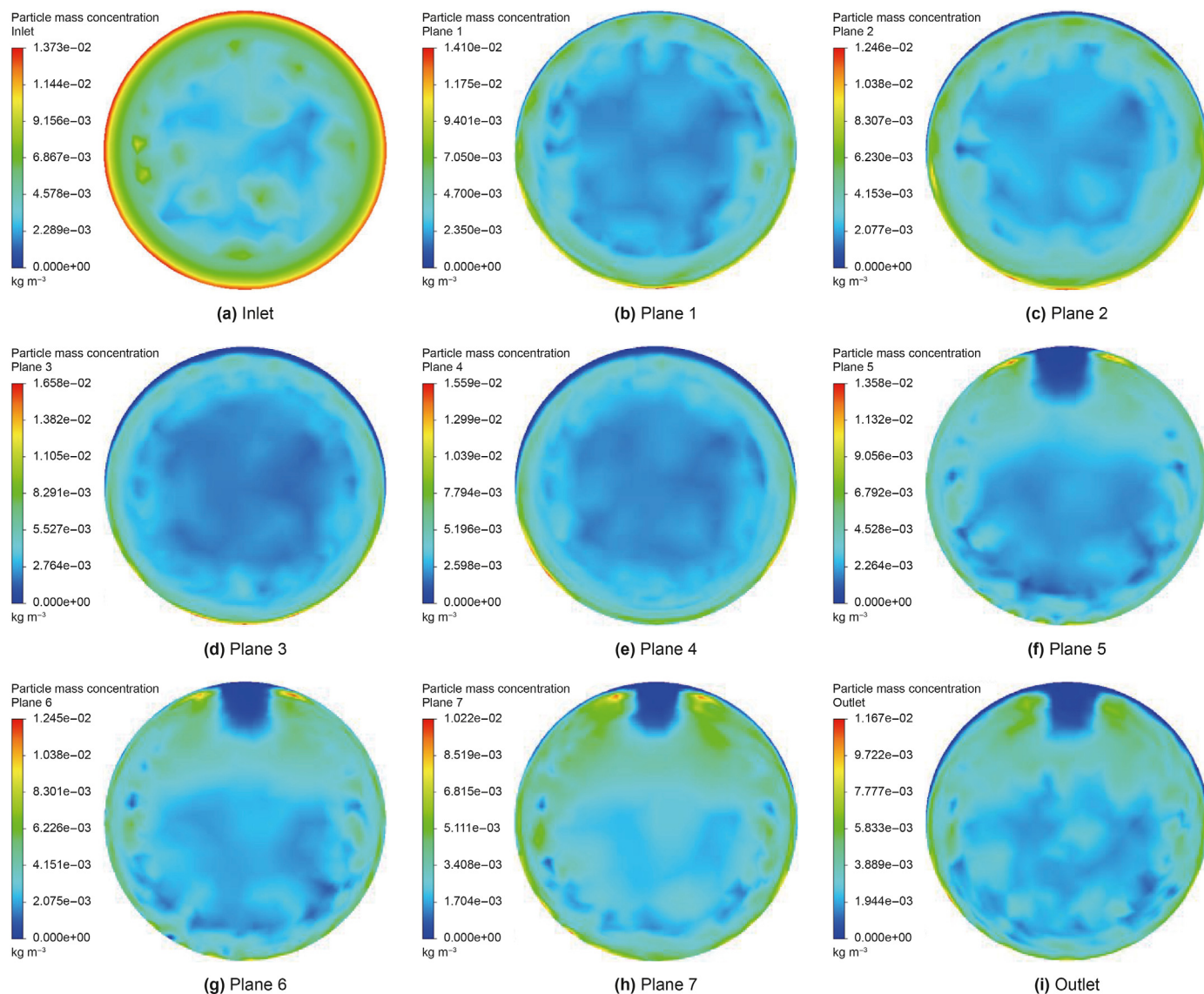


Fig. 11. Concentration distribution of corrosion inhibitor at 15° sections.

concentration of corrosion inhibitor at the top of the pipeline gradually increases, indicating that its corrosion inhibition efficiency is higher. This is because the larger the gas flow rate, the stronger the gas carrying droplet ability, the longer the film forming distance, and the longer the protection distance at the top of the pipeline. Therefore, there is a proportional relationship between the top corrosion inhibitor concentration and the gas flow rate, but the overall trend is to decrease with the extension of the pipeline distance. According to Fig. 17(b), the corrosion inhibitor concentration at the bottom of the pipeline is inversely proportional to the gas flow rate, that is, the lower the gas flow rate, the higher the corrosion inhibitor concentration at the bottom of the pipeline. Under the action of gravity, the particles show a tendency to sediment from the top to the bottom of the pipe. The lower the gas flow rate, the faster the particles settle, resulting in the higher concentration of the corrosion inhibitor at the bottom of the pipe, and the shorter the distance of corrosion inhibitor film formation in the pipe. In this regard, the protective distance of the film within the pipe is reduced.

4.2.4. Influence of filling rate on inhibitor distribution

After the corrosion inhibitor is atomized by the nozzle of the filling port, it is filled into the pipeline at different filling speeds under different pump pressures. In this section, the distribution of the corrosion inhibitor at different filling speeds is analyzed. The inhibitor concentration at each point is shown in Fig. 18.

The concentration of corrosion inhibitor at the top of the pipeline showed an upward trend with the increase in the filling rate. With the increase of the initial velocity of the corrosion inhibitor, its sedimentation velocity decreases and the migration distance increases, extending the protection distance at the top of the pipeline. It can be seen from Fig. 18(b) that the distribution law of the corrosion inhibitor at the bottom of the pipeline is opposite to that at the top. As the distance increases, the overall concentration shows a downward trend, and with the increase of the filling rate, the concentration gradually decreases. Due to the decrease in the filling speed, the initial speed of the droplets is slow, the kinetic energy generated is smaller, the sedimentation speed is faster, and the concentration at the bottom is greater. As a result, there is less concentration in the back part of the pipeline, which is not

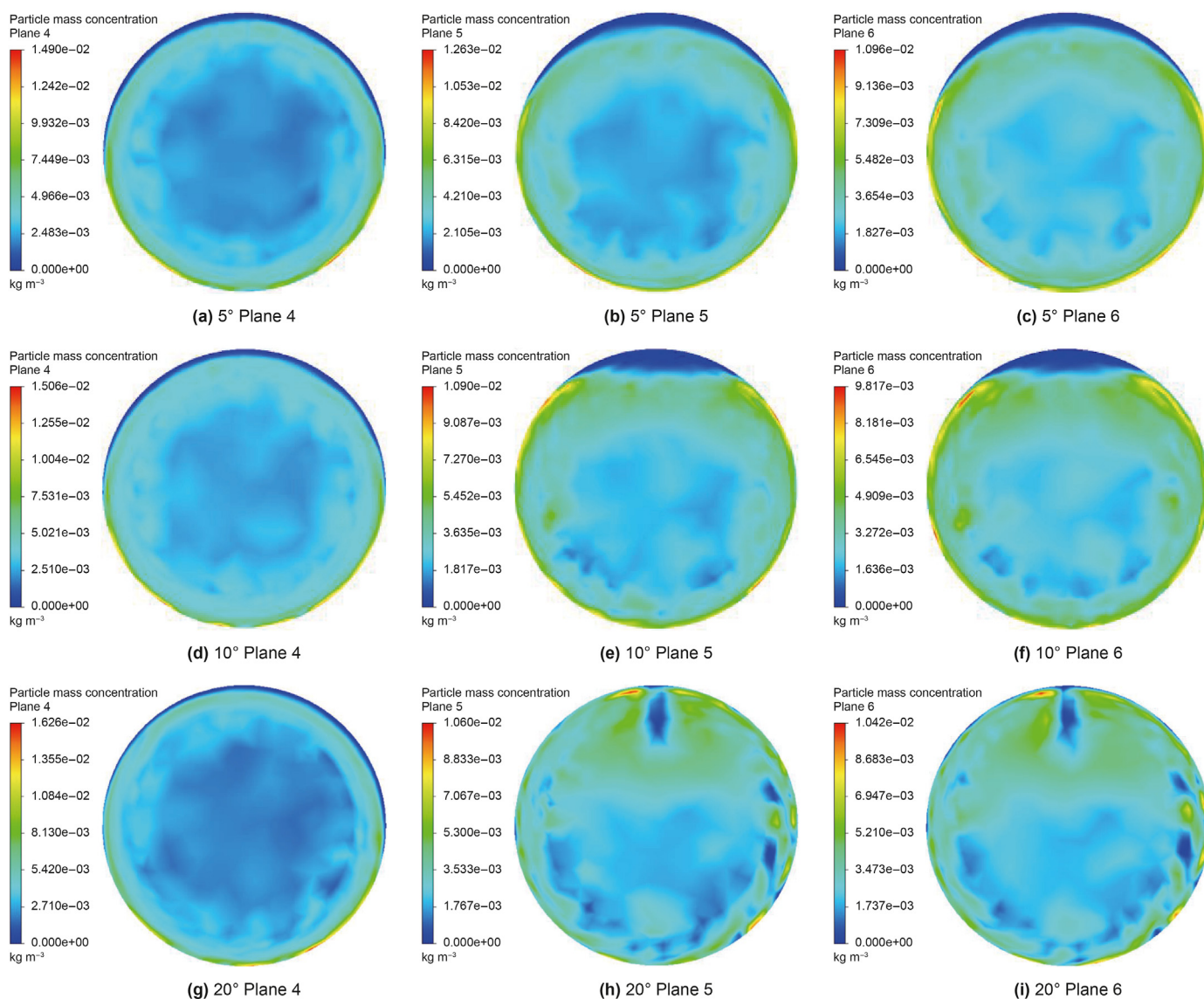


Fig. 12. Cloud map of corrosion inhibitor distribution at different angles.

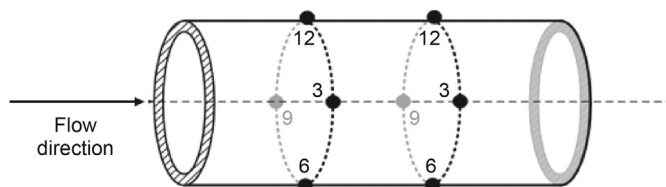


Fig. 13. Schematic diagram of selection rules.

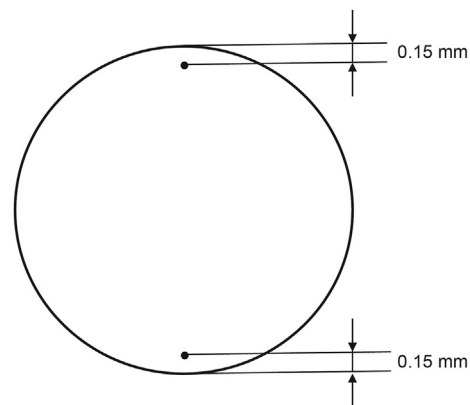


Fig. 15. Schematic diagram of extraction line.

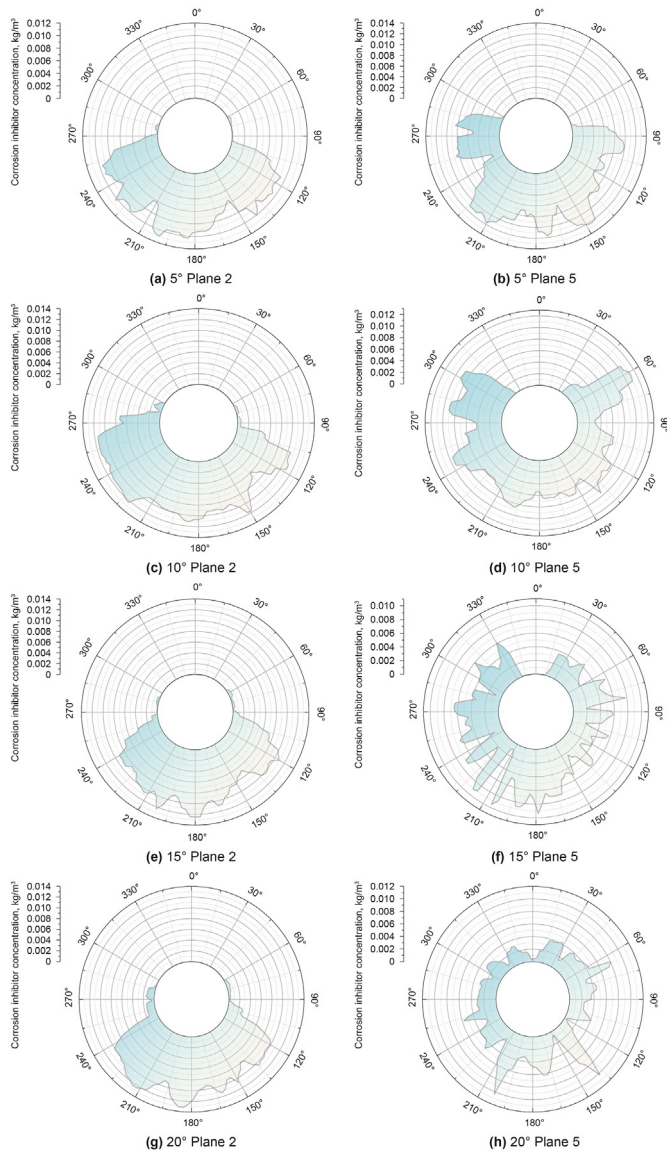


Fig. 14. Circumferential variation of corrosion inhibitor concentration at different angles.

conductive to the film formation of the corrosion inhibitor in the pipeline.

4.2.5. Influence of particle size on the distribution of corrosion inhibitor

The corrosion inhibitor particles are mainly affected by gravity in the pipe and are also affected by the flow of gas in the pipeline. These two factors are related to the distribution of the corrosion

inhibitor. Under different droplet size conditions, the concentration distribution of the corrosion inhibitor at the top and bottom of the pipeline is shown in Fig. 19. At the top of the pipeline, as the particle size increases, the concentration gradually decreases. The larger the particle size of the corrosion inhibitor particles, the more obvious the effect of gravity, and the shorter the distance of the top film formation under the same pipeline conditions.

The distribution law at the bottom of the pipeline is opposite to that at the top. Due to the different degrees of gravity in the pipeline and the gas carrying capacity of different particle sizes in the pipeline, the local variation trend is different. However, in general, as the particle size decreases, the concentration of the corrosion inhibitor at the bottom of the pipeline is lower, indicating that more particles are carried to the back of the pipeline to form a film. Overall, there is an obvious distribution law, that is, the smaller the particle size, the lower the concentration at each point at the bottom, indicating that the smaller particle size settles more slowly, and the longer the film-forming distance is, the more conducive to the distribution of the corrosion inhibitor in the pipe, thus prolonging the protection distance.

By analyzing the influence of different factors on the distribution of corrosion inhibitor in the continuous filling process, it can be seen that the angle of the pipe has the greatest influence, and the front end of the elbow is mainly affected by gravity and gradually settles to the middle and lower parts of the pipeline. After passing through the elbow, with the increase of the angle, the degree of the corrosion inhibitor being carried up also increases, and the better its distribution in the pipe, the more conducive to the formation of the corrosion inhibitor film. For the same pipeline angle, particle size is the main influencing factor. As the carrying capacity of the same gas flow rate is limited, the migration distance of the corrosion inhibitor with a larger particle size is reduced, which is not conducive to the migration of the corrosion inhibitor to the back of the pipeline to form a film. Therefore, it can be analyzed from the perspective of the pipeline during the pipeline design period, and for the pipeline that has been built, the particle size generated by the corrosion inhibitor nozzle can be studied.

4.3. Analysis of corrosion inhibitor filling strategy

With the increase in the operating life of the pipeline, a certain amount of corrosion products will form and scale inside the pipeline, resulting in uneven electrochemical properties of the inner wall of the pipeline which causes local corrosion and perforation. Therefore, when the natural gas gathering and transportation pipeline is put into use and pigging is carried out, the pipeline will

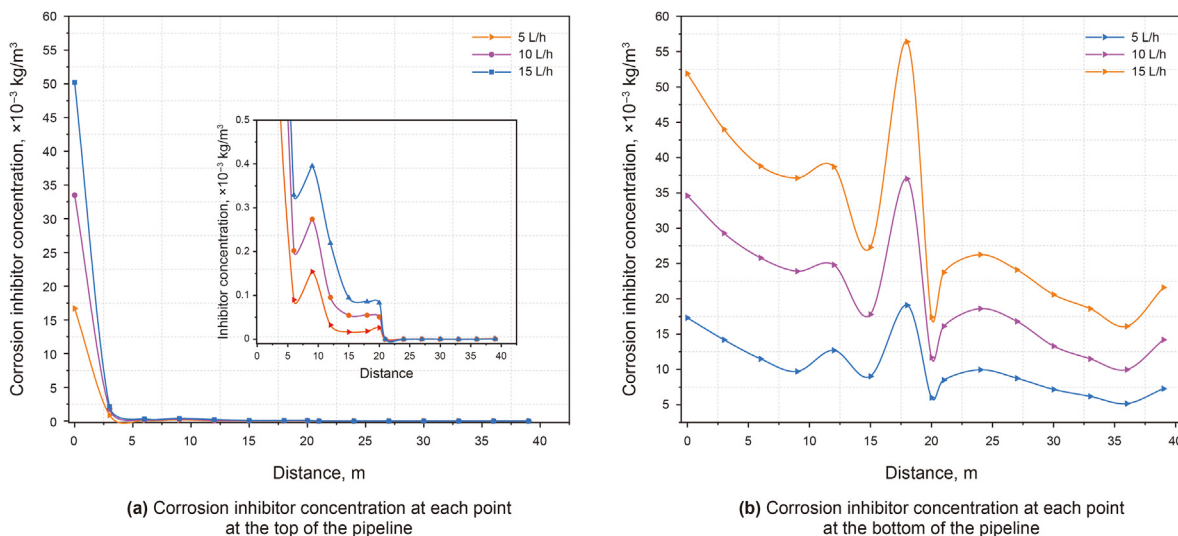


Fig. 16. Concentration map of corrosion inhibitor at each point under different filling volume.

be treated with corrosion inhibitor pre-film, mainly through the pressure difference between the front and rear of the pipeline to move the pig, forming a thin film on the pipe wall. Before calculation, a layer of corrosion inhibitor film is evenly coated on the inner wall of the pipeline by using the patch function of the software. As can be seen from Fig. 20, when the gas flow rate is greater than 4 m/s, the corrosion inhibitor of the pipe wall is seriously damaged, so 4 m/s is selected as the critical flow rate. To quantify the corrosion inhibitor defect at different positions of the pipeline, the data of the corrosion inhibitor volume fraction is extracted according to Fig. 15, as shown in Fig. 21.

It can be seen from Fig. 21 that the volume fraction of the corrosion inhibitor on the wall of the pipeline varies little, the volume distribution of the liquid film is relatively regular, the volume fraction of the corrosion inhibitor in the pipe section fluctuates between 0.8 and 1, and the overall volume can reach more than 0.8, indicating that the irregular turbulent motion of the airflow in the pipe. Since the liquid film will be damaged under the erosion of the pipeline fluid, it is necessary to analyze the loss of the corrosion

inhibitor in the pipeline to determine the loss of the corrosion inhibitor. The loss value is mainly calculated by numerical simulation and innovative self-programming software, as shown in Fig. 22. The loss calculation formula is shown in Equations 11-14.

$$Q_{m1} = \rho A_1 \vec{v}_1 \tag{11}$$

$$Q_{m2} = C_g A_2 \vec{v}_g \tag{12}$$

$$C_g = \frac{Q_{m1} \vec{v}_g}{4\pi D_t X} e^{-\frac{\vec{v}_g}{4D_t X} (r^2 + R_0^2)} I_0 \frac{\vec{v}_g r R_0}{2D_t X} \tag{13}$$

$$A_2 = A - A_1 \tag{14}$$

Where, Q_{m1} is the loss of corrosion inhibitor in the liquid phase, kg/s; ρ is the density of corrosion inhibitor, kg/m³; A_1 is the cross-sectional area of the corrosion inhibitor liquid film at the outlet of the pipeline, m²; \vec{v}_1 is the average flow rate of corrosion inhibitor liquid film at the outlet section of the pipeline, m/s; Q_{m2} is the loss

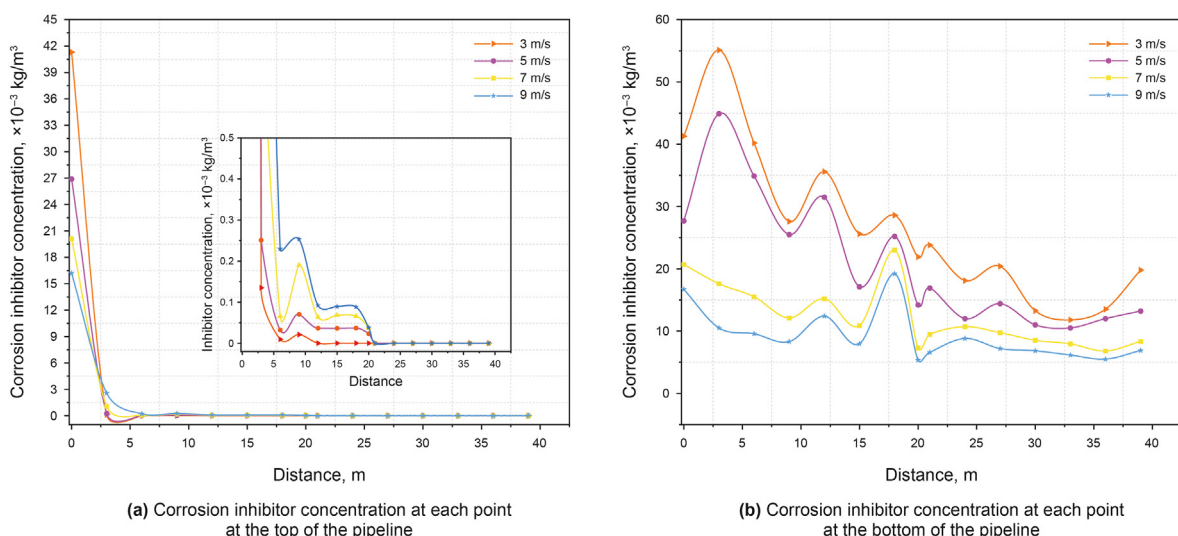


Fig. 17. Concentration of corrosion inhibitor at each point under different gas flow rates.

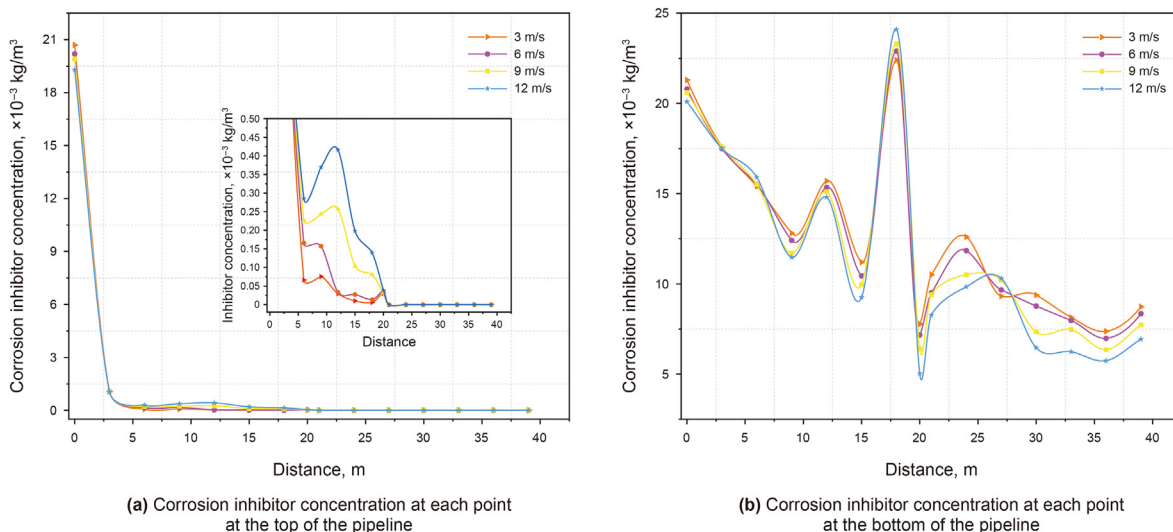


Fig. 18. Corrosion inhibitor concentration at each point at different filling rates.

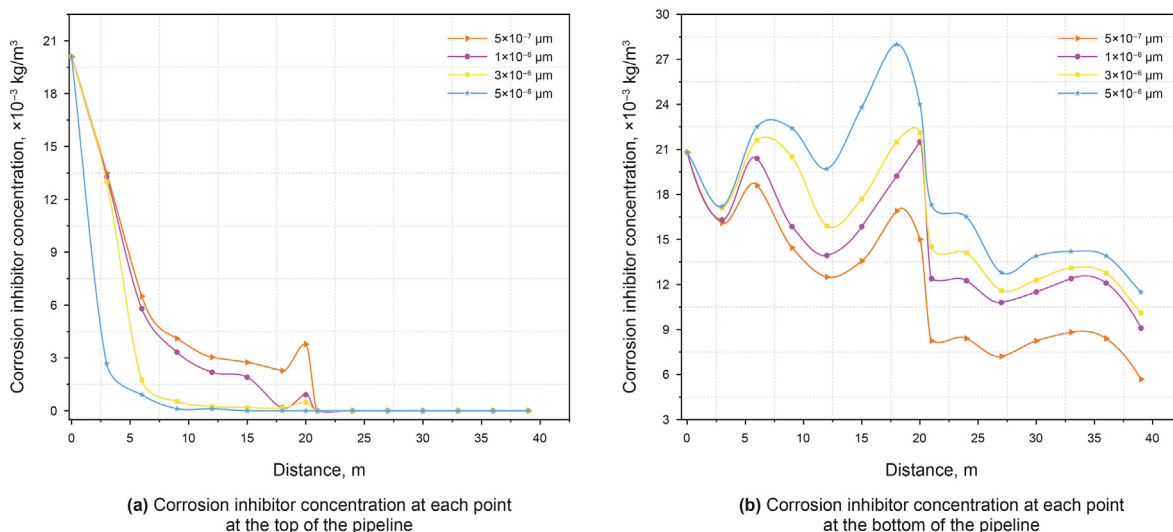


Fig. 19. Corrosion inhibitor concentration at each point under different particle sizes.

of corrosion inhibitor in the gas phase, kg/s ; C_g is the concentration of corrosion inhibitor in gas, kg/m^3 ; A_2 is the flow area of natural gas in the pipe, m^2 ; \bar{v}_g is the gas flow rate, m/s ; D_t is the turbulent diffusion coefficient, m^2/s ; X is the axial distance of corrosion inhibitor movement, m ; r is the radial coordinate, m ; R_0 is the radius of the centrifugal nozzle as an imaginary ring source, m ; I_0 is the first kind of zero order Bessel function; A is the cross-sectional area of the pipe outlet, m^2 .

Through calculation, the corrosion inhibitor loss in the current liquid phase is $5.31 \times 10^{-3} kg/s$, and the loss of corrosion inhibitor in the gas phase is $2.59 \times 10^{-6} kg/s$. Based on the law of mass conservation, it is recommended to increase the filling volume of corrosion inhibitor to 20 L/h to ensure that corrosion inhibitor loss and filling volume are conserved. The filling method of corrosion inhibitor is mainly related to the loss volume and loss time. Through analysis, it is determined that intermittent filling or continuous filling is adopted. For this working condition, the relationship between loss and time under the intermittent filling

process is shown in Fig. 23.

According to the above analysis, when the flow rate is kept within 4 m/s, the integrity of the inhibitor liquid film on the pipe wall is high. It is found that when the volume fraction of the inhibitor fluctuates between 0.8 and 1, the pipeline can be effectively protected. Therefore, taking 0.8 as the critical value of the volume fraction of the corrosion inhibitor, it is considered that when the corrosion inhibitor is lost by 20%, it is necessary to replenish it. Through calculation, it is necessary to fill the inside of the pipeline every 9.5 h, and the filling volume should be greater than 20 L/h. The current filling volume of 6.3 L/h cannot ensure the integrity of the corrosion inhibitor film. Since the loss of the corrosion inhibitor in the liquid phase is $5.31 \times 10^{-3} kg/s$, and the mass flow rate of the 20 L/h filling volume is $5.56 \times 10^{-3} kg/s$, if the filling volume of the corrosion inhibitor is increased to 20 L/h, the use of continuous filling can ensure the continuous integrity of the pipeline corrosion inhibitor film.

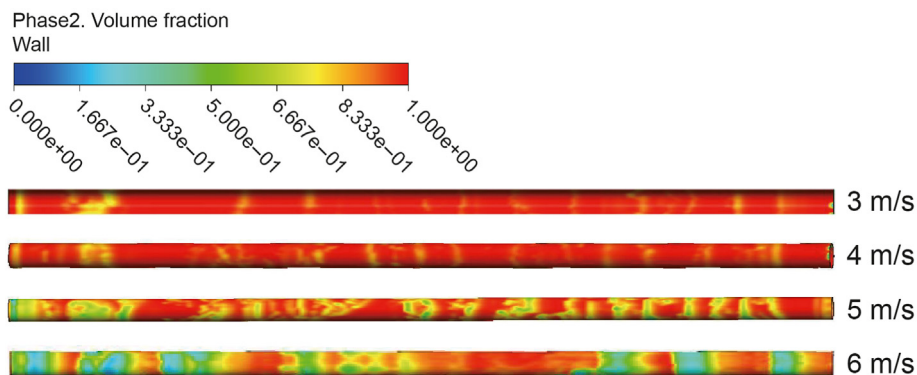


Fig. 20. Volume fraction of corrosion inhibitor under different gas flow rates.

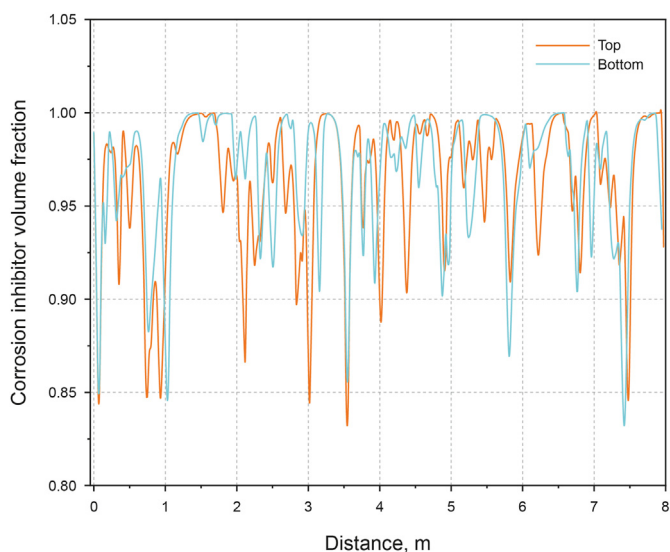


Fig. 21. Corrosion inhibitor volume fraction at different positions.

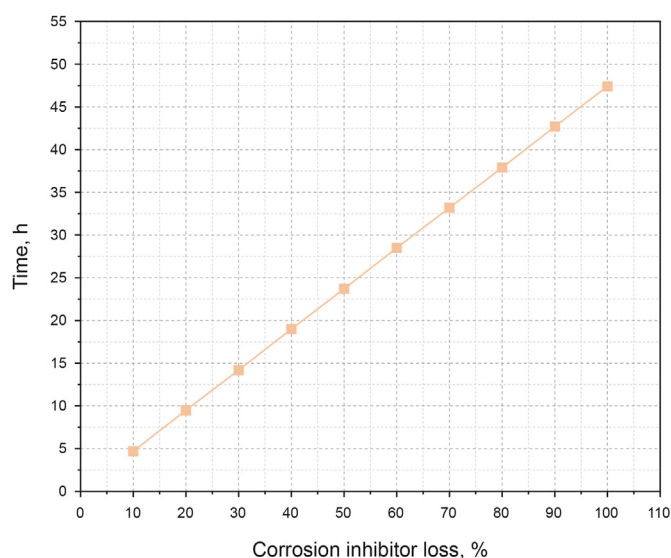


Fig. 23. Correlation between corrosion inhibitor loss percentage and time.

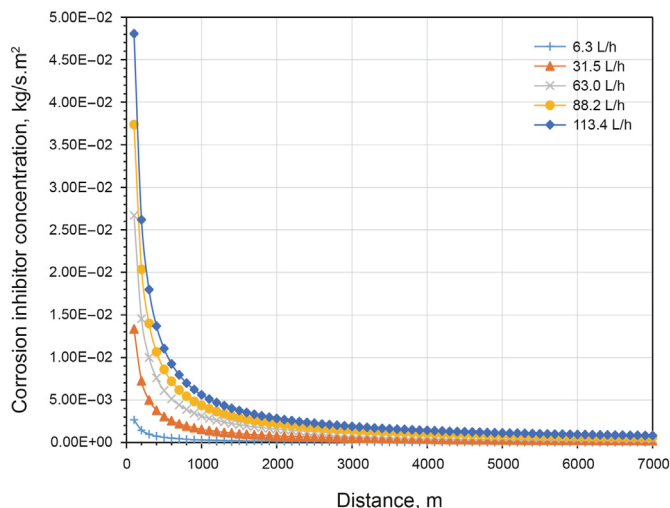


Fig. 22. Changes in corrosion inhibitor concentration under different filling volumes.

5. Conclusion

- (1) Independently design a set of experimental device, which can perform distribution experiments, electrochemical experiments and surface morphology analysis, etc. Through the above experiments, the distribution of corrosion inhibitor in the pipeline, the impedance value at different positions and the corrosion inhibition efficiency and other parameters can be obtained. This device has the advantages of easy measurement, wide application and high simplicity.
- (2) Through the comparative analysis of the parameters measured in the experiment and the numerical simulation model, the correlation degree is more than 80%, and the correlation is high, that is, the simulation results have certain credibility.
- (3) From the simulation results, it can be seen that the distribution law of the corrosion inhibitor is proportional to the gas flow rate, the filling rate, and the pipe angle, and is inversely proportional to the particle size. Specifically, the larger the filling rate, the larger the pipe angle, and the smaller the particle size, the more uniform the corrosion inhibitor is distributed in the pipe. But increasing the filling volume of the corrosion inhibitor will not affect the uniform distribution in the pipe. Since the gas flow rate is

proportional to the shear force, in actual engineering application, the corrosion inhibitor can be uniformly distributed and formed into a film in the pipeline by controlling the particle size, pipeline angle, and filling speed, to achieve the expected effect.

- (4) For the corrosion inhibitor injection strategy, it is mostly determined by empirical methods in the field. In this study, by combining independent programming and numerical simulation, a method to determine the filling method is proposed, which is based on the principle of mass conservation of loss and filling. This method provides some suggestions for the filling volume and filling cycle of corrosion inhibitor in the field.

Declaration of competing interest

The authors declare that they have no known competing financial interests or personal relationships that could have appeared to influence the work reported in this paper.

Acknowledgments

This work was supported by the Sichuan Natural Science Foundation(2023NSFC0422) and the Petrochina's "14th Five-Year plan" Project(2021DJ2804).

References

- Adaze, E., Badr, H.M., Al-Sarkhi, A., 2019. Cfd modeling of two-phase annular flow toward the onset of liquid film reversal in a vertical pipe. *J. Pet. Sci. Eng.* 175, 755–774. <https://doi.org/10.1016/j.petrol.2019.01.026>.
- Bagheri, M., Sari, A., 2022. Study of natural gas emission from a hole on underground pipelines using optimal designbased cfd simulations: developing comprehensive soil classified leakage models. *J. Nat. Gas Sci. Eng.* 102, 104583. <https://doi.org/10.1016/j.jngse.2022.104583>.
- Chen, J.Y., Tang, Y., Zhang, W., et al., 2015. Computational fluid dynamic simulations on liquid film behaviors at flooding in an inclined pipe. *Chin. J. Chem. Eng.* 23 (9), 1460–1468. <https://doi.org/10.1016/j.cjche.2015.07.012>.
- Chen, Y., Wu, H.C., Chen, Y.J., et al., 2022. Erosion-corrosion coupling analysis of shale gas production pipe. *Eng. Fail. Anal.* 138, 106308. <https://doi.org/10.1016/j.engfailanal.2022.106308>.
- Chai, C.X., Xu, Y.H., Xu, Y., et al., 2020. Dopamine-modified polyaspartic acid as a green corrosion inhibitor for mild steel in acid solution. *Eur. Polym. J.* 137. <https://doi.org/10.1016/j.eurpolymj.2020.109946>.
- Cui, L., Hang, M.Y., Huang, H.H., et al., 2021. Experimental study on multi-component corrosion inhibitor for steel bar in chloride environment. *Construct. Build. Mater.* 313, 125533. <https://doi.org/10.1016/j.conbuildmat.2021.125533>.
- Deng, Y.J., Zhang, L., Hou, H., et al., 2019. Modeling and simulation of the gas-liquid separation process in an axial flow cyclone based on the Eulerian-Lagrangian approach and surface film model. *Powder Technol.* 353, 473–488. <https://doi.org/10.1016/j.powtec.2019.05.039>.
- Edelbauer, W., 2017. Numerical simulation of cavitating injector flow and liquid spray breakup by combination of Eulerian-Eulerian and Volume-of-Fluid methods. *Comput. Fluids* 144, 19–33. <https://doi.org/10.1016/j.compfluid.2016.11.019>.
- Farokhipour, A., Mansoori, Z., Saffar-Avval, M., et al., 2020. 3D computational modeling of sand erosion in gas-liquid-particle multiphase annular flows in bends. *Wear* 450–451, 203241. <https://doi.org/10.1016/j.wear.2020.203241>.
- Guo, X.S., Cai, X.Y., Liu, J.L., et al., 2022. Natural gas exploration progress of sinopec during the 13th five-year plan and prospect forecast during the 14th five-year plan. *Nat. Gas. Ind.* 41, 12–22. <https://doi.org/10.1016/j.ngib.2021.08.022>.
- Gupta, V.K., Torrilhon, M., 2016. Reprint of: comparison of relaxation phenomena in binary gas mixtures of maxwell molecules and hard spheres. *Comput. Math. Appl.* 72 (2), 271–287. <https://doi.org/10.1016/j.camwa.2016.04.020>.
- Guan, X.R., Zhao, Y.L., Wang, J.J., et al., 2015. Numerical analysis of quasisteady flow characteristics in large diameter pipes with low liquid loading under high pressure. *J. Nat. Gas Sci. Eng.* 26, 907–920. <https://doi.org/10.1016/j.jngse.2015.07.039>.
- Han, T., Guo, J.X., Zhao, Q., et al., 2022. Insights into the multiple applications of modified polyacrylamide as oilfield corrosion inhibitor and water phase tackifier. *Petrol. Sci.* 19, 397–408. <https://doi.org/10.1016/j.petsci.2022.01.003>.
- Jaya, A., Tiong, U.H., Mohammed, R., et al., 2010. Corrosion treatments and the fatigue of aerospace structural joints. *Procedia Eng.* 2 (1), 1523–1529. <https://doi.org/10.1016/j.proeng.2010.03.164>.
- Jing, J.Q., Xiao, F., Yang, L., et al., 2018. Experimental and simulation study of atomization concentration of corrosion inhibitor in a gas pipe. *J. Nat. Gas Sci. Eng.* 49, 8–18. <https://doi.org/10.1016/j.jngse.2017.10.006>.
- Lee, Y.T., Hong, S.H., Chien, L.H., et al., 2020. Liquid film dispersion on horizontal circular tubes under spray impingement. *Int. J. Heat Mass Tran.* 160, 120223. <https://doi.org/10.1016/j.ijheatmasstransfer.2020.120223>.
- Li, X.H., Chen, G.M., Zhang, R.R., et al., 2018. Simulation and assessment of under-water gas release and dispersion from subsea gas pipelines leak. *Process Saf. Environ. Protect.* 119, 46–57. <https://doi.org/10.1016/j.psep.2018.07.015>.
- Liu, E.B., Peng, Y., Ji, Y.Q., et al., 2022d. Energy consumption optimization model of large parallel natural gas pipeline network: using compressors with multiple operating modes. *Energy Fuels.* <https://doi.org/10.1021/acs.energyfuels.2c02929>.
- Liu, E.B., Li, D.J., Li, W.S., et al., 2021a. Erosion simulation and improvement scheme of separator blowdown system —a case study of changing national shale gas demonstration area. *J. Nat. Gas Sci. Eng.* 88, 103856. <https://doi.org/10.1016/j.jngse.2021.103856>.
- Liu, M.Y., Hu, L.M., 2019. A numerical procedure for estimating the sand erosion of elbows in annular flow with the complete thickness distribution of the liquid film. *Wear* 440–441, 203085. <https://doi.org/10.1016/j.wear.2019.203085>.
- Liu, E.B., Li, D.J., Zhao, W.W., et al., 2022a. Correlation analysis of pipeline corrosion and liquid accumulation in gas gathering station based on computational fluid dynamics. *J. Nat. Gas Sci. Eng.* 102, 104564. <https://doi.org/10.1016/j.jngse.2022.104564>.
- Liu, E.B., Wang, X.J., Zhao, W.W., et al., 2021b. Analysis and research on pipeline vibration of a natural gas compressor station and vibration reduction measures. *Energy Fuels* 35 (1), 479–492. <https://doi.org/10.1021/acs.energyfuels.0c03663>.
- Liu, E.B., Peng, Y., Peng, S.B., et al., 2022b. Research on low carbon emission optimization operation technology of natural gas pipeline under multi-energy structure. *Petrol. Sci.* 19 (6), 3046–3058. <https://doi.org/10.1016/j.petsci.2022.09.025>.
- Liu, E.B., Lian, D.P., Zheng, H., et al., 2022c. Research on abnormal vibration and vibration reduction measures of a natural gas compressor station: a case study of the JYG compressor station. *Energy Fuels* 36 (2), 897–909. <https://doi.org/10.1021/acs.energyfuels.1c03849>.
- Longwell, J.P., Weiss, M.A., 1953. Mixing and distribution of liquids in high-velocity air streams. *Ind. Eng. Chem.* 45 (3), 667–677.
- Luo, S., Wang, H.Z., Gao, Z.Y., et al., 2021. Interaction between high-velocity gas and liquid in gas atomization revealed by a new coupled simulation model. *Mater. Des.* 212, 110264. <https://doi.org/10.1016/j.matdes.2021.110264>.
- Mompean, G., 1998. Numerical simulation of a turbulent flow near a right-angled corner using the speziale nonlinear model with RNG $k-\epsilon$ equations. *Comput. Fluids* 27 (7), 847–859. [https://doi.org/10.1016/S00457930\(98\)00004-8](https://doi.org/10.1016/S00457930(98)00004-8).
- Meeusen, M., Zardet, L., Homborg, A.M., et al., 2020. The effect of time evolution and timing of the electrochemical data recording of corrosion inhibitor protection of hot-dip galvanized steel. *Corrosion Sci.* 173, 108780. <https://doi.org/10.1016/j.corsci.2020.108780>.
- Peng, S.B., Zhang, Z., Liu, E.B., et al., 2021. A new hybrid algorithm model for prediction of internal corrosion rate of multiphase pipeline. *J. Nat. Gas Sci. Eng.* 85, 103716. <https://doi.org/10.1016/j.jngse.2020.103716>.
- Qi, G.Q., Yan, H.X., Qi, D.T., et al., 2019. Analysis of cracks in polyvinylidene fluoride lined reinforced thermoplastic pipe used in acidic gas fields. *Eng. Fail. Anal.* 99, 26–33. <https://doi.org/10.1016/j.engfailanal.2019.01.079>.
- Quan, J.X., Liu, X.F., Wang, C.Y., et al., 2022. A study on corrosion failure of the circulation line with valve openings in atmospheric tower based on CFD. *Eng. Fail. Anal.* 141, 106633. <https://doi.org/10.1016/j.engfailanal.2022.106633>.
- Quentin, L., Nicolas, L., Jerome, H., et al., 2021. On the spreading of high-pressure spray-generated liquid wall films. *Int. J. Multiphas. Flow* 139. <https://doi.org/10.1016/j.ijmultiphaseflow.2021.103619>.
- Rojas, S.F., Ojeda, B.C., 2009. Recent development in derivative ultraviolet/visible absorption spectrophotometry: 2004–2008: a review. *Anal. Chim. Acta* 635 (1), 22–44. <https://doi.org/10.1016/j.aca.2008.12.039>.
- Singh, A., Ansari, K.R., Lin, Y.H., et al., 2019. Corrosion inhibition performance of imidazolidine derivatives for J55 pipeline steel in acidic oilfield formation water: electrochemical, surface and theoretical studies. *J. Taiwan Inst. Chem. Eng.* 95, 341–356. <https://doi.org/10.1016/j.jtice.2018.07.030>.
- Tao, Y.J., Huai, X.L., Guo, Z.Y., et al., 2019. Numerical simulation of spray performance based on the euler-Lagrange approach. *J. Therm. Sci.* 18 (1), 91–96. <https://doi.org/10.1007/s11630-009-0091-8>.
- Verdin, P.G., Thompson, C.P., Brown, L.D., 2014. CFD modelling of stratified/atomization gas-liquid flow in large diameter pipes. *Int. J. Multiphas. Flow* 67, 135–143. <https://doi.org/10.1016/j.ijmultiphaseflow.2014.07.008>.
- Wang, Z., Kong, Y.H., Li, W., 2022. Review on the development of China's natural gas industry in the background of "carbon neutrality. *Nat. Gas. Ind.* 41, 194–202. <https://doi.org/10.1016/j.ngib.2021.08.021>.
- Xu, Y.G., Liu, M.Y., Tang, C., 2013. Three-dimensional cfd-vof-dpm simulations of effects of low-holdup particles on single-nozzle bubbling behavior in gas-liquid-solid systems. *Chem. Eng. J.* 222, 292–306. <https://doi.org/10.1016/j.chemengj.2012.08.021>.

- [jcej.2013.02.065](#).
- Yu, H.M., Jin, Y.C., Cheng, W.M., et al., 2021. Multiscale simulation of atomization process and droplet particles diffusion of pressure-swirl nozzle. *Powder Technol.* 379, 127–143. <https://doi.org/10.1016/j.powtec.2020.10.053>.
- Zeng, L., Zhang, G.A., Guo, X.P., et al., 2015. Inhibition effect of thioureidoimidazoline inhibitor for the flow accelerated corrosion of an elbow. *Corrosion Sci.* 90, 202–215. <https://doi.org/10.1016/j.corsci.2014.10.011>.
- Zheng, Y.G., An, G.L., Peng, R., et al., 1999. Calculation formula and field inspection of corrosion inhibitor concentration and protection distance in natural gas pipeline, 01 *Nat. Gas. Ind.* 113–117+23 (in Chinese).
- Zhong, X.K., Shang, T., Zhang, C.F., et al., 2020. In situ study of flow accelerated corrosion and its mitigation at different locations of a gradual contraction of N80 steel. *J. Alloys Compd.* 824. <https://doi.org/10.1016/j.jallcom.2020.153947>.